metals

MDPI

Article

Weibull Statistical Reliability Analysis of Mechanical and Magnetic Properties of FeCuNb$_x$SiB Amorphous Fibers

Ruixuan Li *, Haiying Hao, Yangyong Zhao and Yong Zhang

State Key Laboratory for Advanced Metals and Materials, University of Science and Technology Beijing, No. 30, Xueyuan Road, Beijing 100083, China; haiying-0823@163.com (H.H.); zhaoyangyongwd@126.com (Y.Z.); drzhangy@ustb.edu.cn (Y.Z.)

* Correspondence: liruixuan1208@163.com; Tel.: +86-010-6233-3073

Academic Editor: K.C. Chan

Received: 16 December 2016; Accepted: 17 February 2017; Published: 28 February 2017

Abstract: Glass-coated $Fe_{76.5-x}Cu_1Nb_xSi_{13.5}B_9$ (x = 0, 1, 2, 3, 3.5) fibers were successfully fabricated by a modified Taylor method. The fibers showed circular morphology and smooth surface with different diameters. The mechanical properties of the fibers were evaluated and the Weibull statistical analysis has been introduced to characterize the strength reliability of the fibers, with the modulus m of the amorphous fibers reaching above 20. The magnetic properties were also studied. Lower coercivity was found for the fibers with amorphous, nanocrystalline, and microcrystalline structures rather than that for the coarse crystalline ones. The glass-coated FeCuNbSiB amorphous fibers have excellent comprehensive performance compared with the other kind of fibers.

Keywords: amorphous fibers; modified Taylor technique; mechanical properties; Weibull statistical analysis

1. Introduction

Fe-based soft magnetic materials have developed recent years. Because of the low cost and their excellent soft magnetic properties—e.g., high saturation magnetization and low coercivity—they have received considerable attention [1]. The glass-coated fibers with a diameter ranging from a few microns to a few hundred microns can be prepared by a Taylor-type technique—i.e., a glass-coated melt spinning method. The preparation process allows the control of microstructures and geometrical characteristics by adjusting the technological parameters, such as the feed-in rate of the glass-tube and the winding speed [2,3]. Previous investigations have focused on the magnetic properties. Most typically, the composition of FeCuNbSiB with trademark "Finemet" is widely studied [4–6] while the studies of the mechanical properties are less reported, relatively. Most of the works focus on the mechanical performance of the amorphous bare fibers. However, the coated-glass offers an advantage of high corrosion resistant, high temperature resistance, and high insulation in many practical applications [7,8]. This paper mainly studies the mechanical and magnetic properties of the glass-coated Fe-based fibers and the effect of structures to those properties.

2. Experiment

The ingots of Fe-based system with the compositions of $Fe_{76.5-x}Cu_1Nb_xSi_{13.5}B_9$ (x = 0, 1, 2, 3, 3.5) (at %) were prepared by arc-melting appropriate amounts of Fe (99.9%), Cu (99.9%), Nb (99.999%), Si (99.95%), and industrial Fe–B alloy (which consists of 78.543 wt % Fe, 20.41 wt % B) under a Ti-gettered argon atmosphere.

The fibers were produced by a modified-Taylor technique as shown in Figure 1 [9,10]. Firstly, about 1 g of master alloy was placed in a closed-end Boron-added Pyrex glass tube with 10 mm in diameter and 1 mm in thickness. Then the tube and alloy are heated by an induction coil to around 1300 °C. Lastly, the softened glass tube is drawn into a fine capillary by a pre-prepared glass bar with cutting-edge and rolled onto a rotating cylinder using a motor coupled to the winding system. A water jet was directed at the fibers in order to enhance the quenching. As the diameter cannot be controlled exactly, the glass-coated Fe-based fibers which have diameters ranging from 10–30 μm have been obtained by the equipment (Figure 2) developed in our group with the experimental parameters controlled into the same. One qualified fiber of each of the five compositions is selected and then they are cut into several pieces for different experiments. Although the measuring error and different influential factors may lead to different diameters even in one fiber, the diameter of each fiber is relatively small and the fibers are all completely cooled. Consequently, the effect of the diameter and the resulting cooling rate can be ignored.

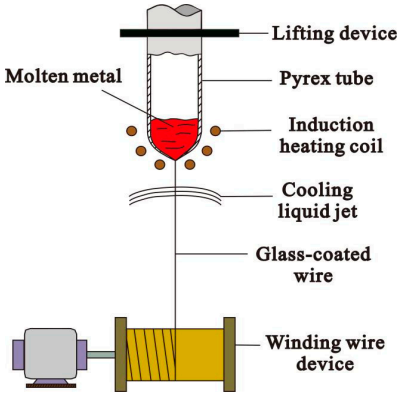

Figure 1. Schematic diagram of the glass-coated melt-spinning process [8,9].

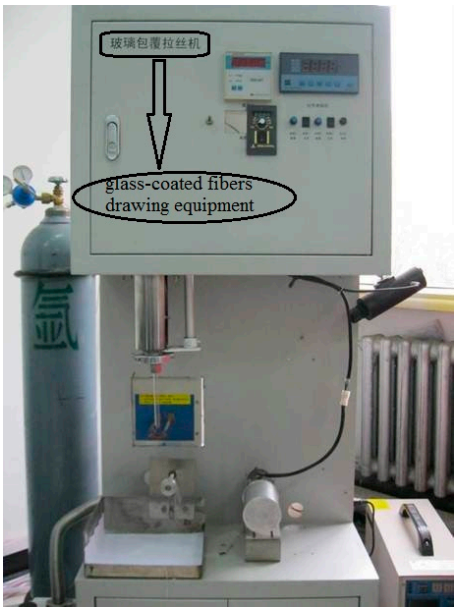

Figure 2. The picture of the glass-coated fibers drawing equipment.

The structure of the five different composition fibers was studied by an X-ray diffraction (XRD, TTRIII, Tokyo, Japan) using Cu K_α radiation. The surface and fracture morphology of the fibers were examined by scanning electron microscopy (SEM, Zeiss Supra 55, Oberkochen, Germany). The tension

tests were performed by using an Instron-5900 machine at room temperature. The gauge length was set as 20 mm and the specimen was elongated at a rate of 1 mm/min. Figure 3 shows the geometry of the tensile sample. The magnetic characterization was carried out using a vibration sample magnetometer (VSM, Quantum Design, San Diego, CA, USA).

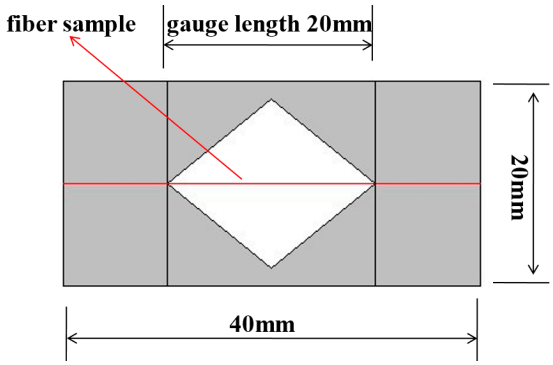

Figure 3. Schematic diagram of the tensile sample.

3. Results

3.1. Surface Morphology and Structure of the Fe-Based Fibers

Figure 4 shows the scanning electron micrograph of typical glass-coated fibers (x = 2) where its composite characteristic can be clearly seen. The fiber shows circular morphology and smooth surface and the glass layer is only 0.5 μm, implying that the modified Taylor technique is very effective in producing the high quality fibers [11,12].

Figure 5 shows the XRD analysis for the different Nb-content fibers. The broadened XRD patterns of x = 0, 2 and 3.5 samples show amorphous nature, while there are BCC α-Fe crystalline peaks in the x = 1 and 3 samples. The degree of crystallization of the x = 1 sample is higher than that of the x = 3 one. Ignoring the effect of diameters, experimental investigations show that the different structures can be related to the composition. It has also been proven that the appropriate experimental parameters, such as the high drawing speed and reasonable cooling water position, tend to form fully amorphous structures [13].

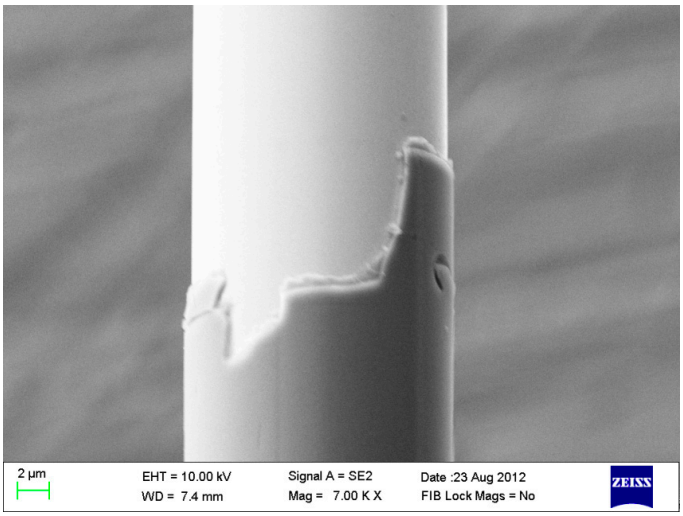

Figure 4. Scanning electron microscopy (SEM) micrographs of the glass–coated fibers (x = 2).

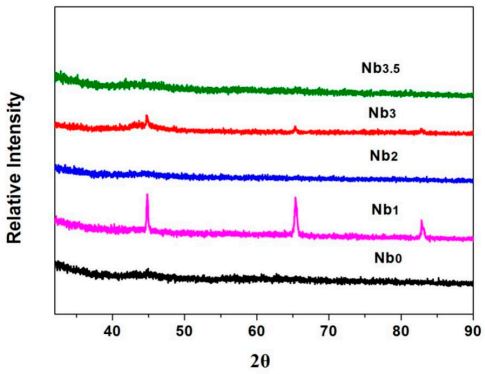

Figure 5. X-ray diffraction patterns of $Fe_{76.5-x}Cu_1Nb_xSi_{13.5}B_9$ (x = 0, 1, 2, 3, 3.5) fibers.

Adding Cu and Nb elements to FeSiB alloy tends to form nanocrystalline structures. Copper can promote the nucleation rate of grains, and Niobium can hinder their growth and make grain distribution homogeneous [14]. It is not certain whether there is nanocrystalline precipitation in the amorphous fibers from the XRD pattern. The longitudinal section morphology of fibers was observed in the SEM. In order to contrast the crystal and amorphous fibers, two group of fibers (x = 0, x = 3) were chosen. Ten fibers of each group were selected and prepared with cool mosaic method. A few hours later, they were burnished using sand paper and mechanical polished. It can be seen that carbon was sprayed on the sample surface. Figure 6 shows the longitudinal section morphology of the fibers (a, x = 3, b, x = 0). It is clear that there are circular crystalline grains generating in the x = 3 fibers and the size of the grain is less than one micron. For the fibers of x = 0, many fine nanocrystalline grains shaped as thin strips can be seen in the amorphous matrix. It is easy to form microcrystalline or nanocrystalline for FeCuNbSiB mircowires produced by the glass-coated melt spinning method.

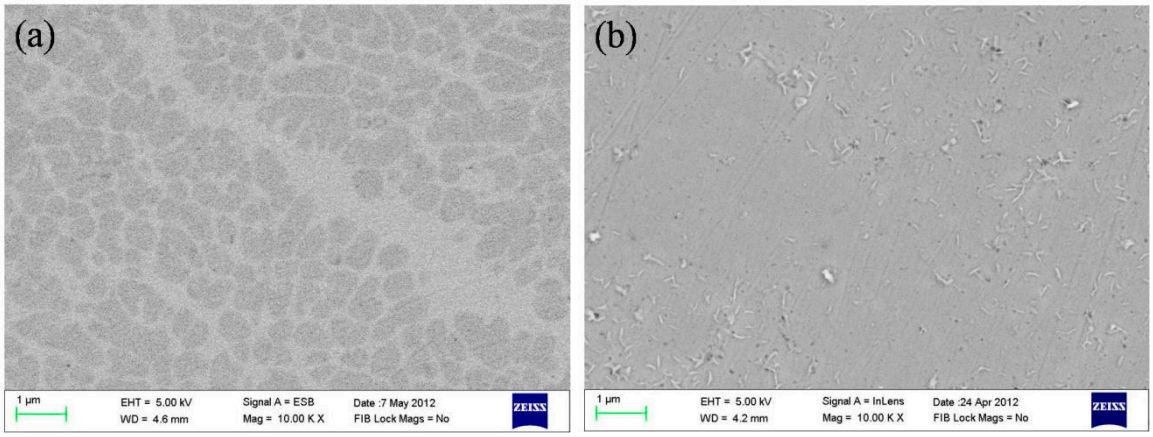

Figure 6. Longitudinal section morphology of fibers (**a**) x = 3 (**b**) x = 0.

3.2. Tensile Tests Analysis

The mechanical properties of the glass-coated fibers were measured in tension tests. Ten samples with relatively the same diameter in each composition were made. The results were obtained by computer automatically. Then five curves in each group with relatively small fluctuation were selected. Figure 7 shows the typical tensile stress-strain curves of $Fe_{76.5-x}Cu_1Nb_xSi_{13.5}B_9$ (x = 0, 1, 2, 3, 3.5) (at %) fibers. There is no plastic deformation stage following the elastic deformation, which identifies typical brittle fracture.

Figure 8 shows the strength distribution of the glass-coated fibers with different content of Nb. The amorphous fibers (x = 0, 2, 3.5) show higher tensile fracture strength between 2.5 GPa to 3.0 GPa

than that of the crystalline ones (x = 1, 3). The fibers of x = 1 show the worst mechanical performance with the tensile fracture reaching about 1.5 GPa and elongation below 2%, as shown in Figure 6b. The tensile strength of the glass-coated amorphous fibers in this test are close to that of general Fe-based bare fibers [15].

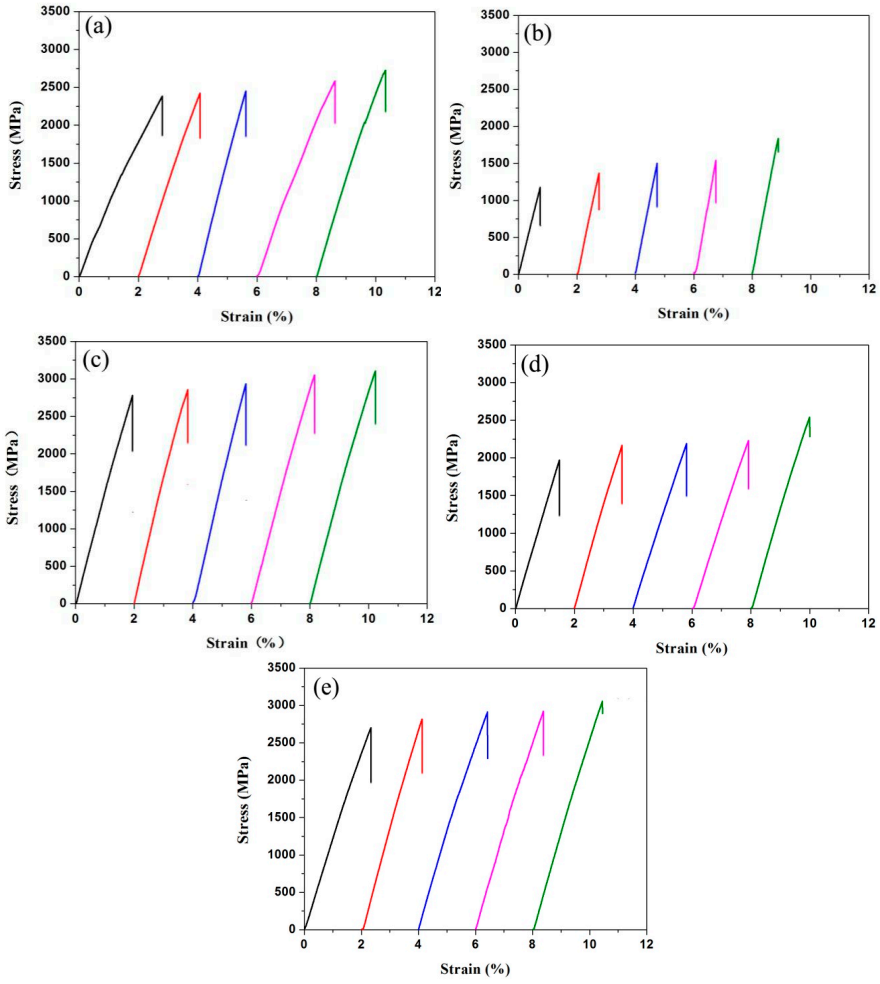

Figure 7. Tensile stress-strain curves of $Fe_{76.5-x}Cu_1Nb_xSi_{13.5}B_9$ fibers: (**a**) x = 0, d = 25 μm; (**b**) x = 1, d = 15 μm; (**c**) x = 2, d = 15 μm; (**d**) x = 3, d = 25 μm; (**e**) x = 3.5, d = 15 μm.

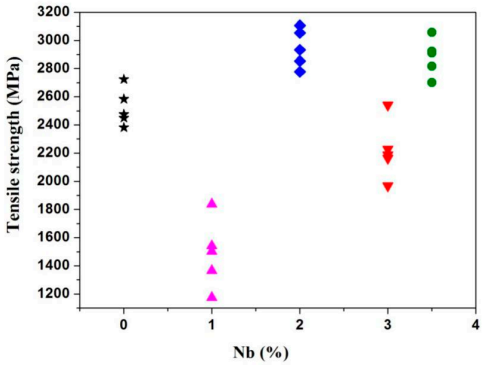

Figure 8. The strength distribution of the glass-coated fibers with different content of Nb.

3.3. Weibull Statistical Analysis

In the tensile tests, we assume that the cross section of the fibers is a perfect circle with uniform diameter. In fact, the fibers inevitably have geometric fluctuation and surface defects. In addition, because of the small sizes of the fibers, it is difficult to ensure that the process of the sample preparation, clamping, and loading operation is completely the same. A fluctuation in fracture strength is observed.

Weibull-statistical analysis has been introduced to characterize the strength reliability of the glass-coated fibers [16–18]. The Weibull equation is usually used to determine the Weibull modulus in the double logarithmic form

$$\ln\{\ln[1/(1-P)]\} = \ln V + m\ln\sigma - m\ln\sigma_0 \quad (1)$$

where m is the Weibull-modulus that represents the strength reliability, σ_0 is a scaling parameter, and V is the volume of the tested samples. P is the fracture probability at a given uniaxial stress, and can be calculated using the equation

$$P_i = (i - 0.5)/n \quad (2)$$

where n is the total number of the samples tested, and i is the sample ranking in ascending order of the failure stress [17].

Figure 9 shows the Weibull plots of the samples calculated by Equation (1). The Weibull plots for the raw data of these samples are represented very well by a linear least-square fit, as can be seen in Figure 9. The Weibull modulus is 20.54, 25.06, and 25.30 for the amorphous fibers (x = 0, 2, 3.5), and is 7.07 and 11.63 for the crystalline ones (x = 1, 3), respectively. The Weibull modulus m actually reflects the reliability of the test samples. A higher m value represents a narrow dispersion of the fracture strength, and thus a higher reliability. The results show that the strength reliability of the amorphous fibers is higher than that of the crystalline ones in the texts. Crystalline fibers which have grain-boundaries and surface defects lead to larger fluctuations in the fracture strength. The m value for the glass-coated amorphous Fe-based fibers in the present study is close to that of the Mg-based [16] and smaller than that of the Co-based [17] and Zr-based amorphous fibers [18].

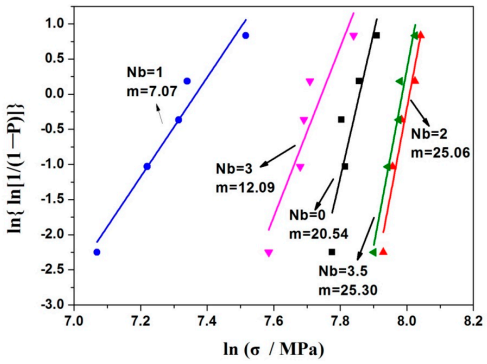

Figure 9. Weibull plots of the tensile fracture strength and corresponding fits to the data for the five types FeCuNbSiB fibers showing an inclined fracture.

3.4. SEM Analysis of Fractured Samples

Figure 10 illustrates the fracture morphology observed in the sample of x = 2. The fracture surfaces exhibit two morphologically distinct zones. One zone is smooth and featureless, while the other is a pronounced vein pattern, as can be seen in the Figure 10a. The tensile fracture angle θ between the tensile axis and the fracture plane can be readily measured on the surface of the sample, as marked in Figure 10b. It is found that the tensile fracture angle θ is equal to 54°, which obviously deviates from the angle of the maximum shear stress plane (45°). The glass layer is only 0.5 μm, which can be seen from Figure 3, only accounting for 5.88% of the total fiber. This phenomenon can easily explain the

reason for the glass-coated Fe-based fibers with such a high tensile strength of about 3 GPa, which is close to the tensile strength of the general Fe-based bare fiber and exceeds that of the glass-coated fibers reported.

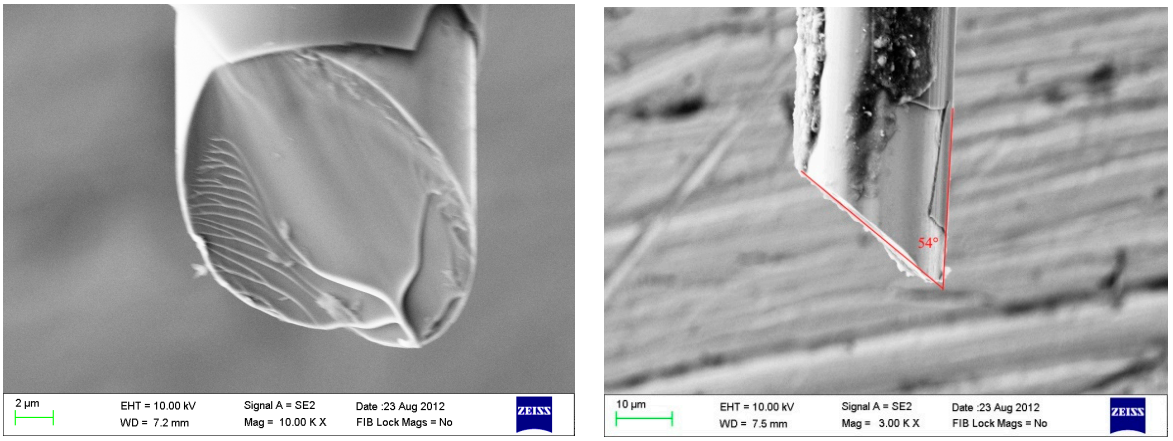

(**a**) (**b**)

Figure 10. SEM micrograph of the fractured samples. (**a**) Fracture surface shows vein pattern; (**b**) fracture angle is about 54°.

3.5. Magnetic Properties of the Samples

The room-temperature hysteresis loops for the five different compositions in the series of $FeCuNb_xSiB$ fibers are presented in Figure 11. As observed, the fibers of x = 0, 3, and 3.5 show long narrow shapes, while the fibers of x = 1 and 2 show nearly rectangular shape and are still not saturated in the applied magnetic field of 500 Oe. It can be inferred that the magnetic behavior is greatly influenced by the composition and structure of the fibers.

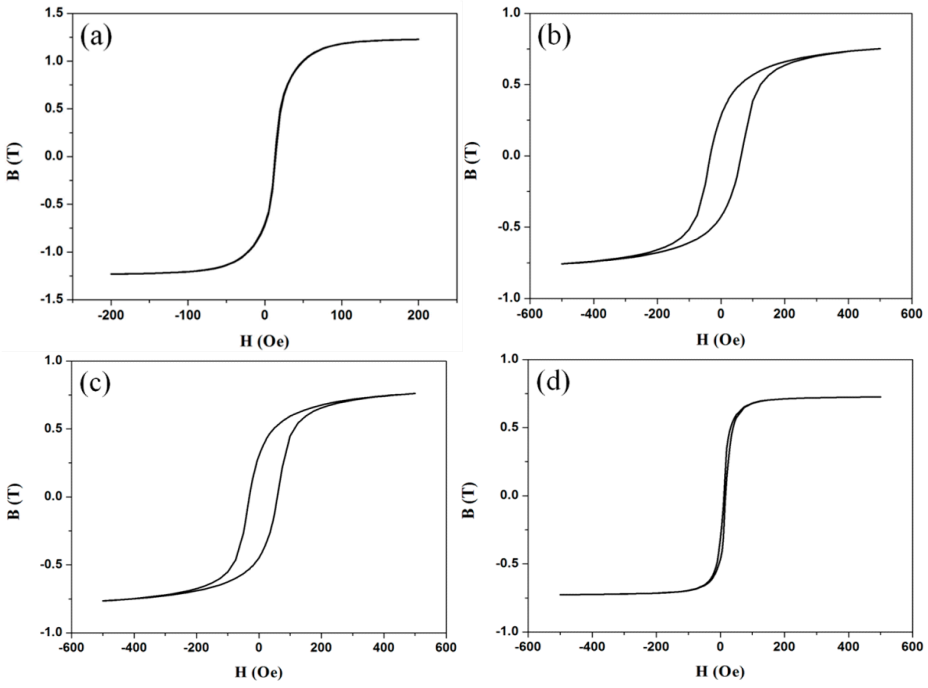

Figure 11. *Cont.*

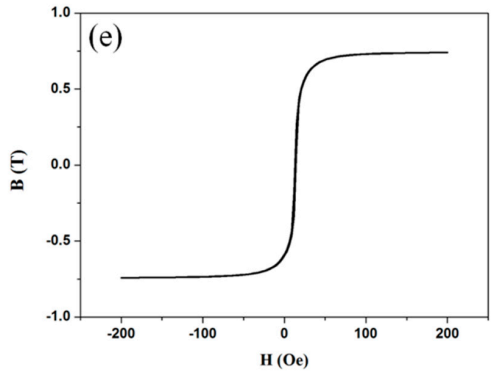

Figure 11. Hysteresis loops of different compositions of $Fe_{76.5-x}Cu_1Nb_xSi_{13.5}B_9$ fibers, (**a**) x = 0, d = 25 μm; (**b**) x = 1, d = 30 μm; (**c**) x = 2, d = 30 μm; (**d**) x = 3, d = 20 μm; (**e**) x = 3.5, d = 15 μm.

The impact of Nb on the saturation induction density Bs, coercivity Hc and remanence ratio Mr/Ms of the Fe-based wires is shown in Figure 12. The coercivity result corresponds to the XRD analysis except the fibers of x = 2. The amorphous fibers exhibit particularly low coercivity value. While in coarse crystalline samples, the value is almost dozens of times more than that of amorphous and nanocrystalline ones, where the major controlling factor is changed and magneto-crystalline anisotropy is reduced. The change rule of remanence ratio Mr/Ms is the same with that of the coercivity. However, the content of Nb has different influence on the saturation induction density. It is clear that the sample of x = 0 shows the highest value of 1.2 T. The remaining samples all show lower value between 0.7 T and 0.8 T.

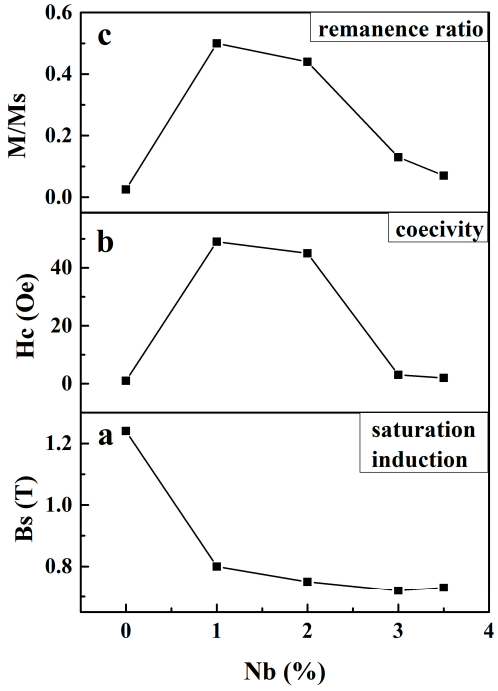

Figure 12. The content of Nb dependence of Bs (**a**), Hc (**b**), and Mr/Ms (**c**).

The effect of the glass layer on the magnetic properties was also studied. The glass was removed by hydrofluoric acid with the mass fraction of 20%. Figure 13 shows the hysteresis loops of the as-cast (x = 3) and glass-removed fibers with the diameters of 30 μm. The coercivity decreased from 3.26 Oe to 1.20 Oe. In the practical applications, we can consider whether to remove the glass or not according to different conditions.

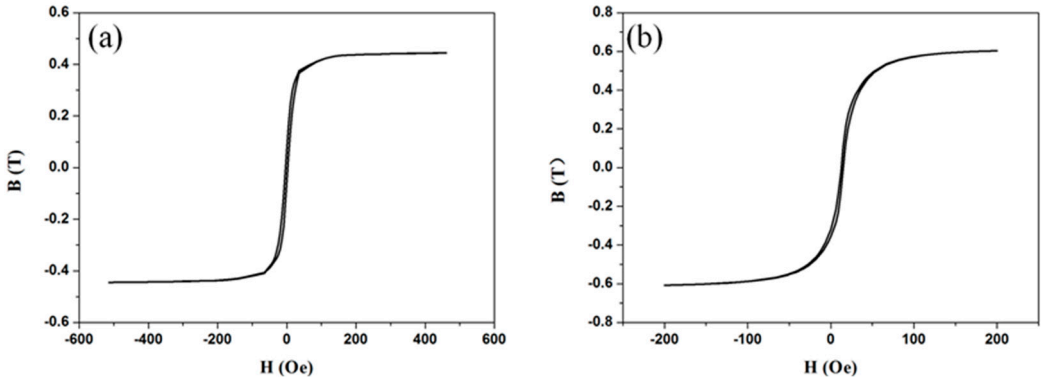

Figure 13. Hysteresis loops of (**a**) as-cast and (**b**) glass-removed $Fe_{73.5}Cu_1Nb_3Si_{13.5}B_9$ fibers.

4. Discussion

It has been verified above that the glass-coated FeCuNbSiB fibers made of modified-Taylor method show excellent properties such as high strength and low coercivity, and the high-strength effect is highlighted especially in amorphous ones. The amorphous fibers have caught much attention for their high fracture strength and toughness. The tension tests of the melt-extracted $Cu_{48}Zr_{48}Al_4$ amorphous microwires were carried out by Sun et al. [19], indicating that the fracture strength ranged from 1724 MPa to 1937 MPa, and the average strength and standard deviation were 1836 MPa and 56 MPa, respectively. In contrast, the strength value is highly improved after the glass coat is added. It should be noted that the glass coats produced by the glass-coated drawing fiber equipment show circular morphology and a smooth surface, which effectively impede the rapid expansion of the shear band in the amorphous phase. As a result, the abrupt failure of one dominant shear band and highly localized deformation can be put off. This can explain the phenomenon of the present glass-coated FeCuNbSiB amorphous fibers exhibiting much higher strength of 2500–3000 MPa.

As for the low-coercivity effect, the microstructure of fibers, combined with the morphology, play an important role. In coarse crystal fibers which have exactly the similar particle sizes to that of the domain wall width, the anisotropies act a pivotal part and impede the magnetic domain wall in rotation or mobility. As for the amorphous or nanocrystalline structure, however, the ferromagnetic exchange interactions start to dominate and thus average out the magneto-crystalline anisotropy which randomly fluctuates on a scale much smaller than the domain wall width [20]. Consequently, there is no net anisotropy effect on the magnetization process, leading to a smaller coercive force value.

In practical application, the glass-coated fibers show such properties as anticorrosion and high-temperature resistance while, when the glass is removed, better soft magnetic property can be obtained. That is to say, the coated-glass also makes great contribution to the lower coercivity, which can be explained by the residual inner stress. The typical characteristic of the glass-coated fibers is that there are great internal stress including radial compressive stress between glass and inner metal core, because of the different coefficient of thermal expansion and the axial tensile stress during the drawing preparation process. The removal of the glass reduces part of the stress in fibers, and thus the distribution of the magnetic domain is changed. With the decrease of radial stress, the radial magnetic domain in the inner core decreases, leaving only the axial domain, while the circular domain in the outer shell increase greatly, as shown in Figure 14. As a result, the magnetic anisotropy is reduced, which in turn leads to a lower coercivity.

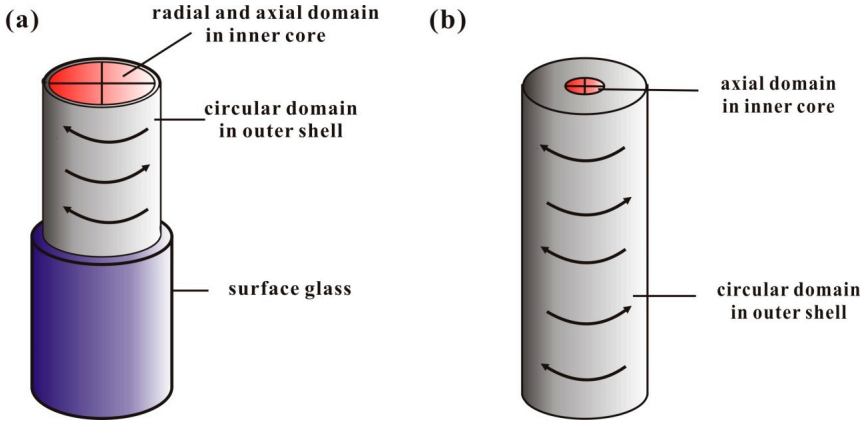

Figure 14. Magnetic domain distribution of (**a**) as-cast and (**b**) glass-removed $Fe_{73.5}Cu_1Nb_3Si_{13.5}B_9$ fibers.

A direct comparison of the tensile strength and saturated magnetization of the FeCuNbSiB alloy system with a different shape is presented in Figure 15. Although having excellent magnetic properties such as high saturation magnetization, the ribbons and the films cannot show high tensile strength, compared with the fibers. In all of the three kinds of fibers, the glass-coated FeCuNbSiB fibers exhibit the most outstanding properties with the combination of relatively high saturation magnetization and high tensile strength, especially for the amorphous one. The saturated magnetization of the amorphous fibers is higher than that of the as-cast and glass-removed fibers and they have excellent comprehensive performance. Consequently, the glass-coated FeCuNbSiB amorphous fibers are of a good choice for the components requirement both for great magnetic and tensile properties.

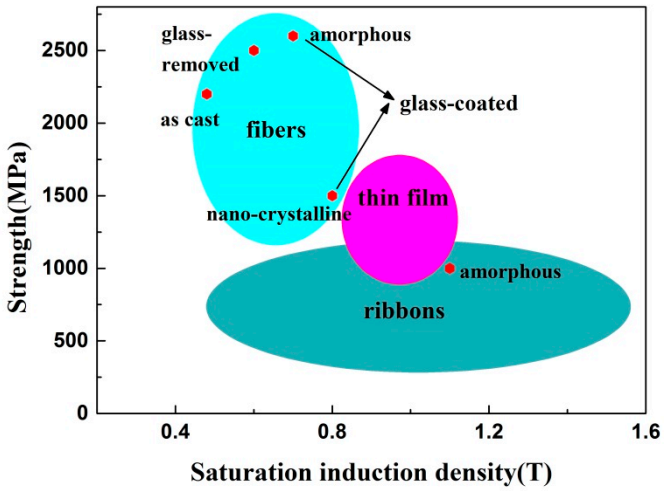

Figure 15. The map of tensile strength and saturated magnetization of the FeCuNbSiB alloy system with different shapes and structures.

5. Conclusions

The mechanical and magnetic properties of glass-coated $Fe_{76.5-x}Cu_1Nb_xSi_{13.5}B_9$ (x = 0, 1, 2, 3, 3.5) fibers prepared by a modified-Taylor method were studied. The main findings of the present work can be summarized as follows:

1. The continuous glass-coated FeCuNbSiB fibers with similar diameters were successfully fabricated by the glass-coated drawing fiber equipment which is developed in our group.

The fibers show circular morphology and smooth surface and the thinnest glass layer is about 0.5 μm.

2. The tensile stress-strain curves show that the glass-coated fibers have a typical brittle fracture. The strength of the amorphous fibers is higher than that of the crystalline ones prepared in this test.
3. Weibull statistical analysis has been introduced to characterize the strength reliability of the fibers. The Weibull modulus *m* of the amorphous fibers reaches above 20, far higher than that of the crystalline ones.
4. The magnetic behavior is greatly influenced by the structure and composition of the fibers. The coercivity of the amorphous or nanocrystalline structure is far lower than that of coarse crystal ones. Compared with all the other kinds of fibers, the glass-coated FeCuNbSiB fibers with the intrinsic amorphous nature have the best comprehensive performance, combining the great magnetic and tensile properties.

Acknowledgments: Yong Zhang would like thank the financial support from National Natural Science Foundation of China (NSFC), granted No. 51471025 and 51671020.

Author Contributions: Haiying Hao, Yangyong Zhao and Yong Zhang conceived and designed the experiments; Haiying Hao and Yangyong Zhao performed the experiments; Haiying Hao and Ruixuan Li analyzed the data; Haiying Hao and Ruixuan Li wrote the paper.

Conflicts of Interest: The authors declare no conflict of interest.

References

1. McHenry, M.E.; Willard, M.A.; Laughlin, D.E. Amorphous and nanocrystalline materials for applications as soft magnets. *Prog. Mater. Sci.* **1999**, *44*, 291–433. [CrossRef]
2. Gotō, T.; Yoshino, A. Mechanical properties and microstructure of high toughness Fe-base filaments produced by glass-coated melt spinning. *J. Mater. Sci.* **1986**, *21*, 1809–1813. [CrossRef]
3. Chiriac, H. Preparation and characterization of glass covered magnetic wire. *Mater. Sci. Eng. A* **2001**, *304–306*, 166–171. [CrossRef]
4. Vázquez, M.; Zhukov, A.P. Magnetic properties of glass coated amorphous and nanocrystalline microwires. *J. Magn. Magn. Mater.* **1996**, *160*, 223–228. [CrossRef]
5. Chin, T.S.; Lin, C.Y.; Lee, M.C.; Huang, R.T.; Huang, S.M. Bulk nano-crystalline alloys. *Mater. Today* **2009**, *12*, 34–39. [CrossRef]
6. Zhukova, V.; Kaloshkin, S.; Zhukov, A.; Gonzalez, J. DSC studies of finemet-type glass-coated microwires. *J. Magn. Mater.* **2002**, *249*, 108–112. [CrossRef]
7. Chiriac, H.; Óvári, T.A. Amorphous glass-covered magnetic wires: preparation, properties, applications. *Prog. Mater. Sci.* **1996**, *40*, 333–407. [CrossRef]
8. Hu, Z.; Liu, X.; Wang, Z.; Xie, J. The rapid solidification prepration and application of glass-coated metallic fibers. *Mater. Rev.* **2004**, *18*, 8–11. (In Chinese)
9. Larin, V.S.; Torcunov, A.V.; Zhukov, A.; Gonzalez, J.; Vazquez, M.; Panina, L. Preparation and properties of glass-coated microwires. *J. Magnet. Magnet. Mater.* **2002**, *249*, 39–45. [CrossRef]
10. Donald, I.W.; Metcalfe, B.L. The preparation, properties and applications of some glass-coated metal filaments prepared by the Taylor-wire process. *J. Mater. Sci.* **1996**, *31*, 1139–1149. [CrossRef]
11. Zhao, Y.; Li, H.; Wang, Y.; Zhang, Y.; Liaw, P.K. Shape Memory and Superelasticity in Amorphous/Nanocrystalline Cu-15.0 Atomic Percent (at. %) Sn Wires. *Adv. Eng. Mater.* **2014**, *16*, 40–44. [CrossRef]
12. Zhang, Y.; Li, M.; Wang, Y.D.; Lin, J.P.; Dahmen, K.A.; Wang, Z.L.; Liaw, P.K. Superelasticity and serration behavior in small-sized NiMnGa alloys. *Adv. Eng. Mater.* **2014**, *16*, 955–960. [CrossRef]
13. Wang, C.D.; Wang, F.M.; Zhang, Z.H.; Xie, J.X. The influence of process parameters on the size, structure and mechanical properties of glass-coated Fe-based fibers. *J. Univ. Sci. Technol. Beijing* **2009**, *31*, 1436–1441. (In Chinese)

14. Herzer, G. Nanocrystalline soft magnetic materials. *J. Magnet. Magnet. Mater.* **1996**, *157/158*, 133–136. [CrossRef]
15. Gotō, T. Fe–B and Fe–Si–B System Alloy Filaments Produced by Glass-Coated Melt Spinning. *Trans. Japan Inst. Metals* **1980**, *21*, 219–225. [CrossRef]
16. Zberg, B.; Arata, E.R.; Uggowitzer, P.J.; Löffler, F. Tensile properties of glassy MgZnCa wires and reliability analysis using Weibull statistics. *Acta Mater.* **2009**, *57*, 3223–3231. [CrossRef]
17. Wu, Y.; Wu, H.H.; Hui, X.D.; Chen, G.L.; Lu, Z.P. Effects of drawing on the tensile fracture strength and its reliability of small-sized metallic glasses. *Acta Mater.* **2010**, *58*, 2564–2576. [CrossRef]
18. Liao, W.; Hu, J.; Zhang, Y. Micro forming and deformation behaviors of $Zr_{50.5}Cu_{27.45}Ni_{13.05}Al_9$ amorphous wires. *Intermetallics* **2012**, *20*, 82–86. [CrossRef]
19. Sun, H.; Ning, Z.; Wang, G.; Liang, W.; Shen, H.; Sun, J.; Xue, X. Tensile strength reliability analysis of $Cu_{48}Zr_{48}Al_4$ amorphous microwires. *Metals* **2016**, *6*. [CrossRef]
20. Herzer, G. Modern soft magnets: Amorphous and nanocrystalline materials. *Acta Mater.* **2013**, *61*, 718–734. [CrossRef]